

*Review*

## A Comprehensive Review on Design and Development of Human Breast Phantoms for Ultra-Wide Band Breast Cancer Imaging Systems

**Ikram E. Khuda**

Iqra University, Defence View, Shaheed-e-Millat Road (Ext), Karachi, Pakistan  
E-mail: ikram@iqra.edu.pk, ikramekhuda@gmail.com

**Abstract.** Microwave ultra-wide band UWB imaging system is a contemporary biomedical imaging technology for early detection of breast cancers. This imaging system requires the development of breast phantoms for experimental data analysis. In order to obtain realistic results, it is very important that these phantoms mimic the characteristics of real biological breast tissue as close as possible. For this purpose, scientists and engineers make use of the dielectric properties of human breast. This paper takes a survey of mathematical formulations used to determine biological dielectric properties and then takes a review of current breast phantoms being used in UWB imaging systems with reference to the analytical dielectric measurements.

At present, breast phantoms are made, both, manually in laboratory utilizing different chemicals and also by using computational electromagnetic algorithms to introduce better heterogeneity in them. They can then easily be tested by doing computer simulations. In this review paper, emphasis is made on the phantoms which are made in laboratory for doing hardware experimentations.

**Keywords:** Microwave, ultra-wideband, biomedical, breast cancer, phantoms, dielectric properties.

**ENGINEERING JOURNAL** Volume 21 Issue 3

Received 30 June 2016

Accepted 17 October 2016

Published 15 June 2017

Online at <http://www.engj.org/>

DOI:10.4186/ej.2017.21.3.183

## 1. Introduction

Breast cancer is one of the most common types of cancers found in women around the globe. These tumor cells most commonly originate in milk ducts of the breast which are composed of epithelial tissues. As illustrated in [1] the manner in which tumor cells propagate indicates whether the tumor is malignant or benign. Benign tumors are considered non- dangerous but certain types of them can cause discomfort and become the reason of breast cancer, as detailed in [2-4]. Malignant tumors have a very high rate of duplication, by virtue of which, they destroy surrounding healthy tissues through a process called metastases [5].

Early detection is a carry out by help of which an individual can identify breast tumors before the symptoms become visible. This could be done clinically using modern instrumentation. In [2] some of the detection measures have been mentioned that must be carried out at different ages among the women. According to these methods, most important is *screening*. Screening refers to tests and examinations which are used to identify a disease, (e.g. cancer in our case) in the people who do not have any symptoms for it. There are different screening tools. Ultra-wideband (UWB) microwave imaging for breast cancer detection has fascinated research awareness as a replacement of prior screening techniques including X-rays, ultrasound and MRI. A brief and adequate comparison for X-ray mammography, MRI and ultrasound testing can be found in [6-9].

In a conventional UWB on body imaging system, a very narrow pulse, in the frequency spectrum of 3.6-10.5 GHz, is transmitted from a UWB antenna to penetrate the target area. As the pulse propagates through the various tissues, reflections and scattering occur at the interfaces. A particular interest is in the scattered signal from a small size-tissue representing a tumor. The reflected and scattered signals can be received using an UWB antenna, or array of antennas, and then it is used to map different layers of the body. As the dielectric properties of tumor differ from healthy breast tissue, this suggests that the reflected and the scattered signals will be different for healthy and affected tissues. Signal processing techniques such as beamforming, hypothesis testing , or time-reversal imaging can then be applied on the received backscattered signal to detect and localize significant scattering regions, such as malignant tumors.

The utilization of electromagnetic (EM) energy in the microwave frequency range is principally smart because it equilibrates the contending necessities for resolution and penetration depth for image processing.

As investigated in [10] and [11], contrast in the dielectric properties between normal and cancerous tissue help in the detection of tumors. Dielectric characteristics of a material are a measure of its ability to interact with electromagnetic (EM) energy and it is a direct consequence of components within the material that can be affected by the electric and magnetic forces generated by the EM fields. In order to test UWB imaging experimentally, models called phantoms of different compositions have been made and tested on the basis of dielectric properties of the real human breast tissue.

To facilitate the development of a communication transceiver system, it is very important to understand channel behavior and its characteristics. In general wireless communication, channels could be free space or faded types. However biological tissue, behave lossy and dispersive characteristics. I.e. their relative permittivity decreases with frequency and simultaneously their conductivity increases. Therefore for experimental purposes, in order to make breast phantoms, it is important to understand the biology and dielectric behavior of the biological tissue (which is under test). These channel characteristics must be taken into account when modeling human breast phantoms.

## 2. The Breast Tissue

In an inclusive view, breast comprises prominently of three types of tissues: breast fat or adipose tissues, glandular tissues and fibrous strands or connective tissues. Glandular tissues lie just below the skin. Glandular tissues consist of lobes with mammary glands in them. These glands terminate into thin tubes called lactiferous ducts. These are ultimately connected to the nipple as an external appearance. Fibrous strands or Coopers ligaments (as they are called) are present to maintain, not only the inner structure of the breast but they also support the tissues to remain attached to the chest walls. The percentage of these tissues is not constant but it varies from individual to individual [12-14]. Water and fat content of these tissues may also vary because of the hormonal activities, like menstruation, pregnancy, lactation and

menopause which occur in different stages of an individual. The inner structure of breast with these tissues is shown in Figs. 1 and 2.

In terms of bio-electrical properties, we have portrayed the human breast in a simplified way, as a combination of four layers. Each layer has its own dispersive and lossy behavior. This layered architecture is made in the order that layer 1 is the outermost layer which envelopes the breast indicating the breast skin. Layer 2 is the fat/ adipose tissues which covers the glandular tissue of the breast. Layer 3 is of glandular tissues in which there are milk ducts present. Tumor cells are mostly present in the membranes of lobules and lactiferous ducts, therefore in our layered model, we will take the fourth layer comprising of tumor cells. This layered structure is shown in Fig. 3. Figure 4 shows three of the most commonly found breast tumors, namely: Ductal carcinoma, lobular carcinoma and lobular carcinoma. The first two are in-situ types and last one is invasive.

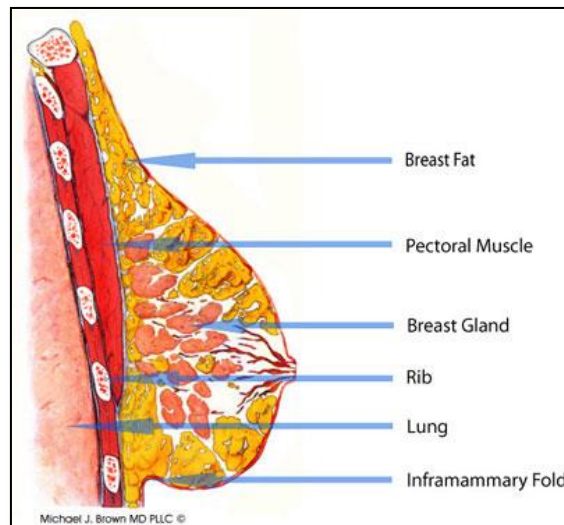


Fig 1. A complex structure of breast tissue showing its anatomy in sagittal view. Image adapted from [15].

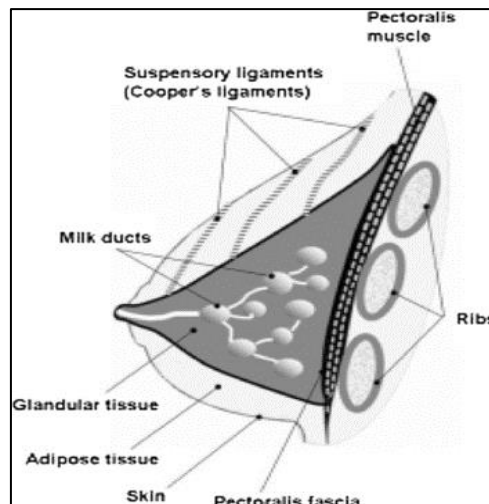


Fig. 2. Simplified view of breast anatomy showing its constituent tissues. Image adapted from [16].

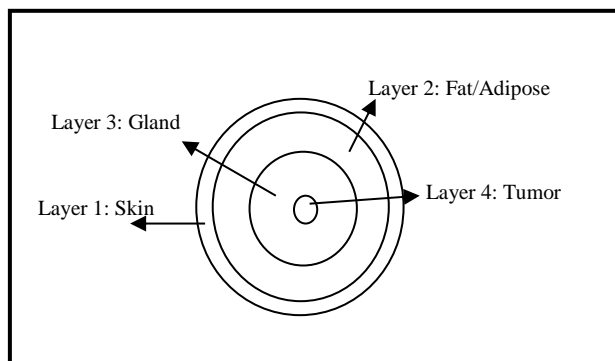


Fig. 3. Layered structure of breast tissue.

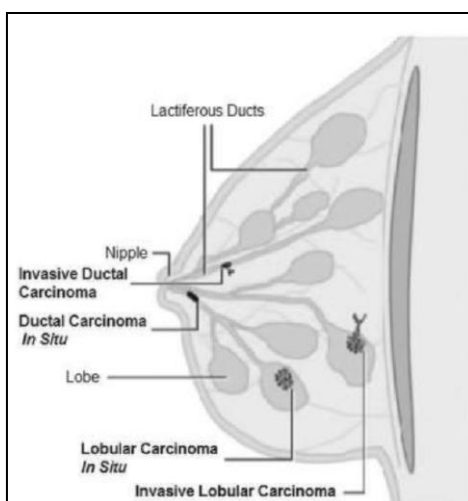


Fig. 4. Sagittal view of breast showing invasive and in-situ tumor locations in it. Image adapted from [15].

### 3. Bioelectric Properties with Associated Mathematics

Bio-electric properties describe the behaviour of biological tissues when subjected to electric and magnetic fields. In general three characteristics define the behaviour of materials in electric and magnetic fields. These are relative electric permittivity ( $\epsilon'$ ) electric conductivity ( $\sigma$ ) and relative magnetic permeability ( $\mu$ ). Human body tissues are non-magnetic materials. The magnetic permeability of biological tissue is taken as that of free space. Therefore the tissues do not have any perceptible consequence on the magnetic field itself. The rapidly changing field only induces electric current in them. When EM waves propagate through a uniform loss less homogenous material, dielectric properties are taken as real number quantities. However if the medium is lossy and does absorb energy, then dielectric properties of the material is obtained from their measured complex relative permittivity,  $\epsilon^*$ , which can be mathematically modeled as shown in Eq. (1) in [17].

$$\epsilon^* = \epsilon' - j\epsilon'' \quad (1)$$

Here  $\epsilon'$  is the real part of complex permittivity of the medium and  $\epsilon''$  is the dielectric loss factor. It is related to the conductivity as in Eq. (2)

$$\epsilon'' = \sigma/\epsilon_0\omega \quad (2)$$

Here  $\sigma$  (S/m) is the total conductivity of the material,  $\epsilon_0$  (F/m) is the permittivity of the free space and  $\omega$  (rad/s) is angular frequency of the fields.

Another common way of writing Eq. (1) is;

$$\varepsilon^* = \varepsilon' - (1 - j \tan \delta) \quad (3)$$

where  $\tan \delta$  is called the loss tangent.

The information obtained from Eq. (1)-(3) is useful in obtaining absorption models of EM waves. The absorption model gives the absorption length which indicates the distance that radiation will propagate through the material before its intensity is markedly decreased. The results state that flux density of EM waves is reduced by a factor of  $e$  ( $e=2.718$ ) as the wave propagates a distance “ $l_a$ ” through the medium. Distance “ $l_a$ ” is called the absorption length.

$$l_a = c/2\omega k \quad (4)$$

Here  $c$  is velocity of EM waves in free space and  $k$  is the wave number.

The response of the medium to an applied time varying field is defined by the relaxation process. Dielectric relaxation is an exponential decay of the polarization in a dielectric medium after the removal of the applied electric field. A relaxation time,  $\tau$  is defined as the instant in which the polarization is decayed to  $1/e$  times its natural value. Here ‘ $e$ ’ is base of natural logarithm. Dielectric relaxation is the source of dispersion, in which dielectric constant decreases as frequency increases. Relaxation time is one of the important considerations when developing human organ phantoms. By the reason of this variation in relaxation time constant, permittivity and conductivity measurements become function of frequency. Therefore phantoms are also to be made frequency dependent, which means that their dielectric properties ought to vary with changing frequencies. Thus in the development of phantoms, we need to consider materials/ ingredients whose dielectric properties match those of the original tissue with the variations in frequency. Figure 5 shows a plot of relative permittivity, conductivity, loss tangent and absorption depth against frequency values in 3.1-11GHz UWB range of microwave frequencies. The parameters values are taken for human breast fat from [17]. Plot is sketched using Scilab ® [18].

Relative electric permittivity gives information on tissues ability to scatter microwave energy and conductivity on the other hand gives information on signal loss as it propagates through the tissue. More is the conductivity; more will be loss due to attenuation and reflection. Research studies also show that relative electric permittivity of tissues are very much dependent on the presence of water; lower the water content lower would be the permittivity and vice versa.

Dielectric relaxation gives the process of dielectric polarization. Usually, polarization of a sample settles down towards the steady state, exemplified by a single relaxation time constant  $\tau$ . The articulation of the dielectric constant for this process was derived by Debye relaxation equation [19] also discussed as single Debye relaxation equation [20]. Debye relaxation is the dielectric relaxation response of an alternating external electric field. It is given as,

$$\varepsilon = \varepsilon_\infty + \frac{(\varepsilon_s - \varepsilon_\infty)}{1 + j\omega\tau} \quad (5)$$

Here  $\varepsilon_s$  and  $\varepsilon_\infty$  are the low and high frequency constraints of the dielectric constant respectively. It is to be noted that Eq. (5) is a single relaxation Debye equation. Process described by Eq. (5) can be separated into real and imaginary parts as follows,

$$\varepsilon' = \varepsilon_\infty + \frac{(\varepsilon_s - \varepsilon_\infty)}{1 + (\omega\tau)^2} \quad (6)$$

$$\varepsilon'' = \frac{(\varepsilon_s - \varepsilon_\infty)\omega\tau}{1 + (\omega\tau)^2} \quad (7)$$

It is notable that we can use relaxation frequency centered on  $f_c$  related to relaxation time  $\tau$  as follows:

$$f_c = 1/(2\pi\tau) \quad (8)$$

Because of the current flow, as group of ions move under the influence of a regular field, the effect of static conductivity,  $\sigma_s$ , is included in the Debye model. Eq. (5) then becomes

$$\varepsilon = \varepsilon_\infty + \frac{(\varepsilon_s - \varepsilon_\infty)}{1 + j\omega\tau} - j \frac{\sigma_s}{\omega\varepsilon_0} \quad (9)$$

Now resolving, Eq. (9) in terms of real and imaginary parts,

$$\varepsilon = \varepsilon_\infty + \frac{(\varepsilon_s - \varepsilon_\infty)}{1 + (\omega\tau)^2} - j \left[ \frac{(\varepsilon_s - \varepsilon_\infty)\omega\tau}{1 + (\omega\tau)^2} + \frac{\sigma_s}{\omega\varepsilon_0} \right] \quad (10)$$

The real and imaginary parts in, Eq. (10) can be compared correspondingly with the real and imaginary parts of (1). At a special case of  $f = f_c$ ,  $\omega\tau = 1$  and Eq. (10) becomes,

$$\varepsilon = \frac{(\varepsilon_s + \varepsilon_\infty)}{2} - j \left[ \frac{(\varepsilon_s - \varepsilon_\infty)}{2} + \frac{\sigma_s}{\omega\varepsilon_0} \right] \quad (11)$$

Interestingly, we see that the real part is mean value of low frequency (or static) and high frequency permittivity. And the imaginary part is a value which is half way in-between static and infinite frequency permittivity plus the static conductivity. With no static conductivity existence, it will be just the half way between. So now we have,

$$\varepsilon' = \frac{\varepsilon_s + \varepsilon_\infty}{2} \quad (12a)$$

and

$$\varepsilon'' = \frac{\varepsilon_s - \varepsilon_\infty}{2} \quad (12b)$$

For a medium that possess non-linear relaxation process, Cole-Cole mathematical formulation is then used [21].

$$\varepsilon = \varepsilon(\omega) = \varepsilon_\infty + \frac{(\varepsilon_s - \varepsilon_\infty)}{1 + (j\omega\tau)^{1-\alpha}} - \frac{\sigma_s}{j\omega\varepsilon_0} \quad (13)$$

$$\varepsilon'(\omega) = \varepsilon_\infty + (\varepsilon_s - \varepsilon_\infty) \frac{1 + (\omega\tau)^{1-\alpha} \sin\left(\frac{1}{2}\alpha\pi\right)}{1 + 2(\omega\tau)^{1-\alpha} \sin\left(\frac{1}{2}\alpha\pi\right) + (\omega\tau)^{2(1-\alpha)}} \quad (14)$$

$$\varepsilon''(\omega) = (\varepsilon_s - \varepsilon_\infty) \frac{(\omega\tau)^{1-\alpha} \cos\left(\frac{1}{2}\alpha\pi\right)}{1 + 2(\omega\tau)^{1-\alpha} \sin\left(\frac{1}{2}\alpha\pi\right) + (\omega\tau)^{2(1-\alpha)}} \quad (15)$$

Exponent parameter  $\alpha$ , in the above equations, takes a value between 0 and 1, which allows describing different spectral shapes. When  $\alpha = 0$ , the Cole-Cole model cuts down to the Debye model. For biological materials  $\alpha$  ranges between 0.3 to 0.5. Cole-Cole relaxation represents a singular case of Havriliak-Negami relaxation when the proportion parameter ( $\beta$ ) is equal to 1 - that is, when the relaxation peaks are symmetric. Another special case of Havriliak-Negami relaxation ( $\beta < 1$ ,  $\alpha = 0$ ) is known as Cole-Davidson relaxation [22, 23].

Debye function in Eq. (5) and Cole-Cole model in Eq. (13) can be expanded to additional terms as well depending upon the different relaxation constant values.

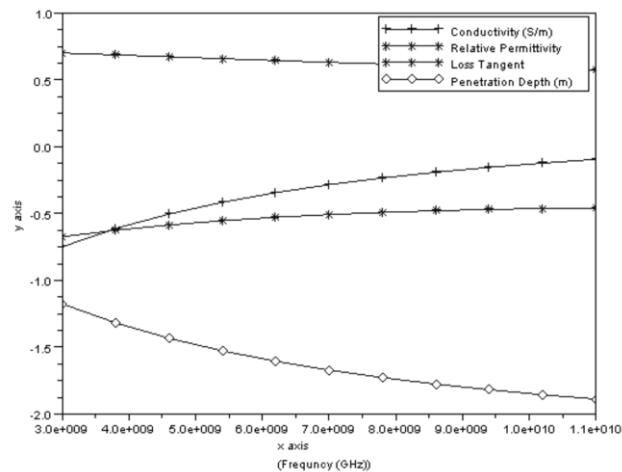


Fig. 5. Relationship of conductivity, relative permittivity, loss tangent and penetration depth for UWB microwave frequency range. Vertical axis is logarithmic.

#### 4. Survey of Dielectric Measurements of Breast Tissue

After taking a quick survey of the mathematical description of dielectric properties in the previous section, we shall now survey upon the measurement results obtained to determine the values of permittivity and conductivity for breast tissues. Considering the layered structure in Fig. 2, we shall survey upon the results obtained so far for the individual layers/ or tissues of breast. . In the cases where dielectric data of human tissues is entailed, it has become regular practice to predict the values of permittivity and conductivity using standard Debye and Cole-Cole functions, as stated in the previous section.

##### 4.1. Results of Dielectric Measurements for Skin

Skin is unavoidably taken of utmost priority because being the outmost layer it is the most exposed portion to the incident fields. Therefore it is expected to absorb most of it. In the research study, to model the characteristics of human skin, permittivity of water is used a major precursor. The reason is that, skin has a water content of 60-70% [24-26]. However it is to be kept in mind that properties of human skin will not be identical as that of water and it also varies in different regions of the body [20].

Mashimo et al [27] have used the two-term Debye function expressed in Eq. (16) to find relative permittivity value of human skin as follows:

$$\text{Re}(\epsilon^*) = \epsilon' = \epsilon_{\infty} + \frac{\Delta\epsilon_l}{1+(\omega\tau_1)^2} + \frac{\Delta\epsilon_h}{1+(\omega\tau_2)^2} \quad (16)$$

where:

$\Delta\epsilon_l = 17.9$  i.e. low frequency relaxation time =  $\epsilon_s - \epsilon_{\infty}$ ;

$\Delta\epsilon_h = 15.0$  i.e. high frequency relaxation time =  $\epsilon_s - \epsilon_{\infty}$ ;

$\epsilon_{\infty} = 3.97$ ;

$\tau_1 = 1.18$  ns  $\rightarrow$  corresponding to low frequency relaxation of 134.87 MHz;

$\tau_2 = 7.1$  ps  $\rightarrow$  corresponding to high frequency relaxation of 22.416 GHz.

The results obtained from above were well fit for a frequency range of 10 MHz to 10GHz. Gabriel et al [17] has published a comprehensive review of measured dielectric properties of human tissues up to 20 GHz using 4 pole Cole-Cole model. A 4 pole equation is obtained by expanding last term on the right hand side of Eq. (13) to four coefficient values of  $\tau$  and  $\alpha$ . This is shown in Eq. (17) as follows:

$$\epsilon(\omega) = \epsilon_{\infty} + \sum_{m=1}^4 \frac{\Delta\epsilon_m}{1+(j\omega\tau_m)^{1-\alpha_m}} + \frac{\sigma_s}{j\omega\epsilon_0} \quad (17)$$

Walters et al [28] have utilized this model to predict the permittivity of dry skin equal at millimeter wave frequency (MMW) to be 5.8-j7.5 at 94GHz.

England et al [29] and Cook [30] experimentally determined the permittivity of human skin from breast using waveguide and coaxial line method respectively. England [29] measured the permittivity for three frequencies at 3.0, 9.4 and 23.6 GHz at 37°C. Normally 37°C is the temperature used for measurements because it is the temperature of human artery blood. England's results were:

$$\begin{aligned}\epsilon^* &= 43.5 - j16.5 @3.0 \text{ GHz} \\ \epsilon^* &= 35.5 - j13.0 @9.4 \text{ GHz} \\ \epsilon^* &= 23.0 - j13.0 @23.6 \text{ GHz}\end{aligned}$$

Cook [30] proposed a single term Debye function to fit the measured data having following parameter values:

$$\epsilon_s = 42, \epsilon_\infty = 4.0, \tau = 6.9\text{ps and } \sigma_s = 0.014\Omega/\text{cm}$$

The result is valid between 1.76GHz to 4.68 GHz at 37°C.

We shall determine the permittivity of human skin using single relaxation Debye function following the approach used by [31]. The single relaxation Debye function of Eq. (9) is repeated here for convenience.

$$\epsilon = \epsilon_\infty + \frac{(\epsilon_s - \epsilon_\infty)}{1 + j\omega\tau} - j \frac{\sigma_s}{\omega\epsilon_0}$$

In order to solve this equation we define the following parameters and their values:

Relaxation frequency ( $f_c$ ): the relaxation frequency of ure water at 37°C according to [32] is 36% of 24.4 GHz which is 8.78 GHz. If the temperature is taken to be 20°C then relaxation frequency is 36% of 17.1 GHz which 6.16 GHz. Infinite permittivity ( $\epsilon_\infty$ ) previously used values for pure water is 4.0 at 37°C and 4.3 at 20°C. These values are obtained from Gabriel et al. [17]. Static permittivity ( $\epsilon_s$ ) is according to value of  $\epsilon'$  taken at 1/10<sup>th</sup> the relaxation frequency. According to Gabriel et al [17] and Alabaster [31] these values for dry skin and wet skin are 36 and 43 respectively. Static conductivity ( $\sigma_s$ ) is set to be zero. This is because deionized water has zero static conductivity. This is the assumption taken in Gabriel et al [17] and Alabaster [31] and is also followed here.

The modelled results at three frequencies in UWB band are presented in Table 1. Using, Eq. (2) corresponding values of conductivities can be determined from the results obtained in Table 1. This new set of values is shown in Table 2. Next we used single pole Cole-Cole model of, Eq. (13) to determine the permittivity and conductivity of skin. Therefore rewriting, Eq. (13), we have

$$\epsilon(\omega) = \epsilon_\infty + \frac{(\epsilon_s - \epsilon_\infty)}{1 + (j\omega\tau)^{1-\alpha}} - \frac{\sigma_s}{j\omega\epsilon_0}$$

Using the same parameter values, just take  $\alpha=0.3$ , as mentioned previously the results obtained are shown in Table 3 and Table 4 for permittivity and conductivity values. Both sets of values of permittivity and conductivity (from Debye and Cole-Cole models) are equally true and can be used to model skin for breast phantoms.

## 4.2. Dielectric Measurements for other Breast Tissues

Like skin, experimental measurements have been made for finding dielectric properties for other three tissue types, namely, fat/ adipose, glandular and tumors. In chapter 5 of Campbell [33] dielectric data is presented for human breast tissue. By using cavity perturbation technique, in vitro dielectric measurements were made on female human breast tissues. A large set of data was gathered from good number of specimen. The results in this study contain data ranges and best preferences of values for modeling of normal and diseased breast tissue. The best choices of values are obtained using Debye dispersion relation and by statistical modelling. These values are reproduced here in Table 5 for reference.

Lazebnik et al. [14] studied the dielectric properties of a normal breast tissue and in [34] the study was extended to dielectric properties of normal, benign and malignant breast tissues. In both of these studies, data were mapped to Cole-Cole model. In these studies normal breast tissue included adipose, glandular and fibroconnective tissues in varying percentages. In the first study [14] it was found that higher the adipose content lower is the dielectric properties and higher the fibroglandular content than higher is the permittivity and conductivity values as compared to previous results. Lazebnik concluded existence of large heterogeneity in normal breast tissue. In the second study [34] she found the differences between normal breast, benign and malignant tumors. Normal breast comprised of adipose, glandular and fibroconnective tissues. Benign tumor tissue included fibroadenoma, cysts and malignant tumor included ductal and lobular carcinomas. It was found that dielectric properties may vary with different frequencies. In both these studies, besides obtaining other useful conclusions in dividing the tissues across a wide frequency range of 0.5-20 GHz, a very detailed data base of dielectric properties was obtained to develop numerical breast phantom models. The dielectric permittivity and conductivity obtained for a human breast at 5 GHz were in a wide range of 4.4-48 and 0.02-4.5 respectively.

Table 1. Permittivity values for dry and wet skin in UWB microwave frequencies using single relaxation Debye equation.

Frequency (GHz)	Dry Skin 37°C	Wet Skin 37°C	Dry Skin 20°C	Wet Skin 20°C
4.5	29.34-j12.98	34.88-j15.83	24.97-j15.09	29.54-j18.44
6.5	24.67-j15.30	29.13-j18.65	19.23-j15.83	22.61-j19.32
8.5	20.51-j15.99	24.13-j19.48	15.21-j15.06	17.62-j18.38

Table 2. Conductivity (S/m) values for dry and wet skin in UWB microwave frequencies using single relaxation Debye equation.

Frequency (GHz)	Dry Skin 37°C	Wet Skin 37°C	Dry Skin 20°C	Wet Skin 20°C
4.5	2.40	2.92	2.91	3.56
6.5	2.96	3.61	3.28	4.01
8.5	3.25	3.97	3.35	4.09

Table 3. Permittivity (F/m) values for dry and wet skin in UWB microwave frequencies using single relaxation Cole-Cole equation.

Frequency (GHz)	Dry Skin 37°C	Wet Skin 37°C	Dry Skin 20°C	Wet Skin 20°C
4.5	31.88-j9.59	37.98-j11.69	28.97-j11.66	34.42-j14.24
6.5	28.77-j11.84	34.19-j14.44	24.85-j13.13	29.39-j16.035
8.5	25.79-j13.01	30.56-j15.87	25.53-j13.39	25.34-j16.35

Table 4. Conductivity (S/m) values for dry and wet skin in UWB microwave frequencies using single relaxation Cole-Cole equation.

Frequency (GHz)	Dry Skin 37°C	Wet Skin 37°C	Dry Skin 20°C	Wet Skin 20°C
4.5	3.25	3.96	3.78	4.62
6.5	3.83	4.67	3.96	4.84
8.5	4.00	4.88	3.77	4.60

Table 5. Permittivity and Conductivity values in UWB microwave frequencies for different types of breast tissues. The table is obtained from [33].

<b>Tissue Type</b>	<b>Parameter</b>	<b>Range of Data</b>	<b>Best Values</b>
<b>Fat</b>	<b>Permittivity</b>	2.8-to-7.6	4-to-4.5
	<b>Conductivity (mS/cm)</b>	0.5-to-2.9	1.1-to-1.4
	<b>% water by weight</b>	11-to-31	15-to-23
<b>Glandular</b>	<b>Permittivity</b>	9.8-to-46	10-to-25
	<b>Conductivity (mS/cm)</b>	3.7-to-34	3.5-to-10.5
	<b>% water by weight</b>	41-to-76	45-to-50
<b>Benign Tumor</b>	<b>Permittivity</b>	15-to-67	10-to-50
	<b>Conductivity (mS/cm)</b>	7-to-49	10-to-40
	<b>% water by weight</b>	62-to-84	60-to-90
<b>Malignant Tumor</b>	<b>Permittivity</b>	9-to-59	45-to-60
	<b>Conductivity (mS/cm)</b>	3-to-43	30-to-40
	<b>% water by weight</b>	66-to-79	75-to-80

## 5. Research Review of Breast Phantoms

Results obtained from mathematical formulations of Debye and Cole Cole models, as mentioned in the previous sections have been used for the making breast phantoms. In the past decade phantom making has been accomplished both manually and by using computer simulations using numerical methods. This section provides a review on phantoms used and developed over the past decade for experimentations on UWB breast cancer imaging.

As mentioned in Section II, human breast is taken to comprise of fat/adipose, glandular and fibro-connective tissues. The same should be taken into account to develop a realistic phantom. Design and development of a breast phantom, as used in the researches in [35-50], includes the following common methodology:

- Selection of materials and making their mixture to imitate a real breast.
- Measurements of the dielectric properties (of the mixture obtained in step a), i.e. relative permittivity and conductivity.
- Authentication of the properties (obtained from step b) with real tissues and from the values provided by Debye and Cole-Cole models.
- Formation of the phantom using the samples prepared in the above steps.
- The shape of the phantom mould used most commonly is either spherical or cylindrical.

For making realistic breast phantom which consists of low water composition adipose tissues, higher water composition glandular tissues and cancerous cells, the breast phantom materials are needed to have the following features:

- They must be capable to simulate the dielectric properties of human breast traversing the whole UWB frequencies range (3.1 GHz-10.6 GHz).

- b) The heterogeneity of the phantoms must be consistent with time without the risk of their mechanical and electrical properties changing..

## 6. Hardware Breast Phantoms

Klemm et al. [35] conducted the experiments with UWB imaging system in the frequency range of 3-10 GHz. They made inhomogeneous breast phantoms, operable at 3 GHz for their system. They used polythene powder and water mixture to make the dense center of the breast. The breast phantom was composed of several different dense tissue materials. Tumor size was taken to be 10 mm. Besides inhomogeneous materials, the breast phantom also included a homogeneous skin, as well as normal breast tissue comparable liquid. The skin layer used was 2 mm thick and it was a part of an 86-mm-radius hemisphere phantom mold. The skin layer was made dispersive, and at 3 GHz, skin had a relative dielectric constant of about 35 and attenuation of 5 dB/cm.

Klemm et al. [35] does not describe the making of different tissue layers and their mixing process. In addition the tumor size detected is very large in the heterogeneous phantom. The real mettle would had been to detect small tumors with high dielectric permittivity values in contrast to comparable permittivity value of the heterogeneous breast. The phantom results have also not been validated with clinical tests. Three experimentations with different percentage of dense tissue were carried out The imaging system developed using this phantom is shown in Figs. 6, 7 and 8. Their consideration details and investigation outputs are summarized in Table 6.

Table 6. Relative permittivity results at 3 GHz from [35].

Type of Phantom	Relative Permittivity @ 3 GHz	Tumor Size Detected	Breast Phantom Dense ?
Adipose Tissue	10		
Glandular Tissue	20-30	10 mm	Yes
Skin	$35 \pm 1$		
Tumor	50		

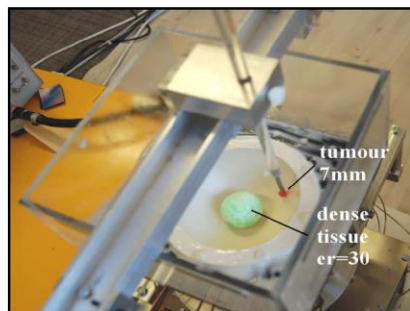


Fig. 6. Picture of the setup of the imaging system 1 from [35].

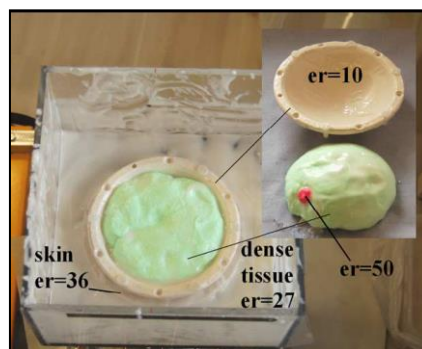


Fig. 7. Picture of the setup of the imaging system 2 from [35].

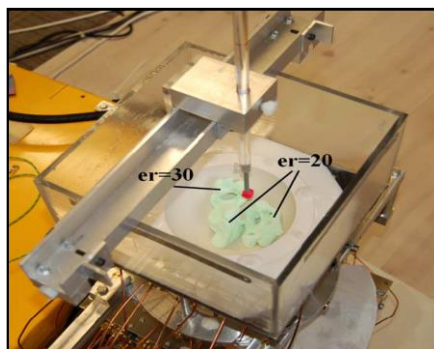


Fig. 8. Picture of the setup of the imaging system 3 from [35].

Lai et al. [36] very comprehensively discussed fabrication of homogeneous and heterogeneous breast phantoms to be used at a frequency range of 0.5-13.5 GHz. They made use of oil and gelatin dispersions proposed by Lazebnik et al. [14] to make phantoms. Phantom materials with different concentrations of oil and water (occupying 400 ml in volume) were produced in cylindrical polypropylene containers. Using the dimensions of 8 cm height and 10 cm diameter homogenous breast phantoms were fabricated in cylindrical polypropylene containers. Oil with 50%, 65% and 80% concentrations were used to make 3 homogenous phantoms. In order to avoid water going to the bottom of the phantom, they were turned upside-down every for every thirty minutes. This procedure was repeated for every 6 hours after fabrication. Seven different heterogeneous phantoms were developed with different volumes of oil. Clutters were made of material with low percentage of oil to simulate the glandular tissue, whereas matrix to hold the clutters was made of materials with high percentage of oil to simulate the adipose tissue in human breast. Clutters were prepared by mincing the high dielectric phantom material to size smaller than 5 mm. Dielectric measurements were made one week after the fabrication of phantoms. Thus it was shown that homogeneous and heterogeneous breast phantoms could be successfully fabricated with oil-in-gelatin dispersion materials. They achieved tumor detection of 4 mm inside the breast phantom. The tumor was made of phantom material with 10% oil. Consideration details for homogeneous phantoms and for heterogeneous phantoms are shown in Table 7 and Table 8 respectively.

Table 7. Homo-80: Homogeneous phantom with 80% oil. Homo-65: Homogeneous phantom with 65% oil. Homo-50: Homogeneous phantom with 50% oil [36].

Breast Phantom Type	Mean Dielectric Permittivity at 5 GHz
Homo-80	8
Homo-65	16
Homo-50	24

Table 8. Compositions of seven heterogeneous breast phantoms of Lei et al. [36].

Breast Phantom Type	Mean Dielectric Permittivity @ 5GHz	Volume of Oil in Clutters	Volume of Clutters in Phantom	Volume of Oil in Phantoms	Tumor Size Detected
Hetero-17	10	50%	17%	75%	4 mm placed inside the breast phantom
Hetero-25	11	50%	25%	73%	
Hetero-33	13	50%	33%	70%	
Hetero-50	16	50%	50%	65%	
Hetero-60	13	70%	50%	75%	
Hetero-65	11	65%	50%	73%	
Hetero-70	10	60%	50%	70%	

Lai et al. [37] extended their previous work in [36], by considering pulse based UWB microwave imaging system and using plastic containers of 10cm diameter and 8cm height as skin. This experimental setup is reproduced here in Fig. 9. The basic shortcoming of their research, Lai et al [36-37], as also mentioned by them is the hardware limitation to detect millimeter sized breast tumors in breast phantoms having higher dielectric properties. Therefore no results are available for tumor size as low as 2mm and 1mm with high malignancy. As a result, it is an experimental system. The results obtained on the phantom have not been testified with clinical tests.

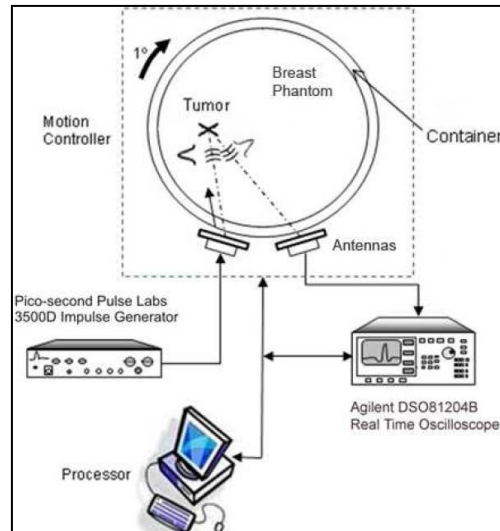


Fig. 9. Experimental setup using in [36, 37].

Alshehri.S et al. [38] presented fabrication of homogeneous and heterogeneous breast phantoms, (operable in 3.1-10.6 GHz UWB frequency range) using easily available materials. The developed breast phantom comprised of four parts: Tumor, fat, skin and glandular tissue. They found that pure petroleum jelly can serve as a homogeneous fatty breast tissue. According to them, skin dielectric properties must lie between those of fatty breast and tumor. This homogeneous phantom developed by them is shown in Fig. 10. They developed three different tumors with different relative permittivity values. To make the breast heterogeneous, glandular tissues were added, having dielectric properties greater than of fatty breast tissues. Soy oil and water-to-wheat ratio in 25.5% of water was used to mimic glandular tissues. The developed heterogeneous phantom model developed by them is shown in Fig. 11. Their consideration details are summarized in Table 9.



Fig. 10. Homogeneous breast phantom developed in [38]. Image is adapted from [38].



Fig. 11. Heterogeneous breast phantom developed in [38]. Image is adapted from [38].

Table 9. Summary of the compositions of heterogeneous breast tissue materials at 6 GHz as used in [38].

Tumor Composition							
Tumor Type	Percentage of Water and Wheat-Flour	Relative Permittivity @ 6 GHz		Conductivity (S/m) @ 6 GHz			
Benign	35.1%	13.4		2.8			
Undefined	55.3%	21.2		4.0			
Malignant	28.4%	56		8.6			
Breast Phantom							
Breast Part	Material Used	Mass (g)		Relative Permittivity @ 6GHz		Conductivity (S/m) @6GHz	
Fatty Breast Tissue	Vaseline	152.3		2.36		0.012	
Skin	Glass	N.A		3.5-10		Insignificant	
Glandular Tissue	Soy Oil and Wheat-Flour Ratio (in 25.5% water)	Soy Oil	Wheat-Flour Ratio	Soy Oil	Wheat-Flour Ratio	Soy Oil	Wheat-Flour Ratio
		76.1	57	2.7	6.98	0.061	0.785

This research paper also presented other possibilities of same and different materials with different ratios and percentages that could be used for making phantoms.

Alshehri, S. A. and Khatun, S et al. [39] developed a feed forward neural network (NN) to identify the existence and location of tumor tissue in a breast model. This work was done using UWB signals at 4 to 8 GHz center frequencies range. A hemisphere shaped breast model based on their previous research in [38] was chosen with four parts, comprising of skin, fat, chest and tumor. The used dielectric properties that were used are shown in Table 10 here.

Table 10. Dielectric Properties at 4 GHz for the phantom components in S. A. Alshehri et al. [39].

Breast part (Including Tumor)	Relative Permittivity @ 4 GHz	Conductivity (S/M) @ 4 GHz	Tumor Size Detected
Skin	37.9	1.49	2.5 mm
Fat	5.14	0.14	
Chest	53.5	1.85	
Tumor	50.0	1.20	

Alshehri, S. A. and Khatun, S et al. [40] proposed a VNA free prototype for UWB imaging systems using methodology developed in [38, 39] to build homogeneous and heterogeneous breast phantoms. Tumor is made by controlling water content percentage in the complete water-wheat and flour blend. A specific glass is used as skin. This is a VNA free prototype. Satisfactory results were obtained for tumor detection with size and localization. The results were verifiable in the whole UWB frequency range of 3.1-10.6 GHz. The experimental setup is shown in Fig. 12.

Shortcomings of the research conducted by, Alshehri, S. A. and Khatun, S et al. [38-40], was that firstly it is an experimental system. It is not tested and verified by clinical testing. Secondly the experiments were conducted at 4.7 GHz. No results could be obtained at higher frequencies because of the hardware limitations. Thirdly only benign tissues were considered for tumor identification. Moreover variations in benign tumors were also not considered. This shows the incapability of the system to differentiate between comparable dielectric properties between glandular breast tissue and malignant breast tumor. Fourthly the permittivity and conductivity values taken here are not indicated for which temperature gradient taken, as shown Debye and Cole-Cole models, in Section 2.

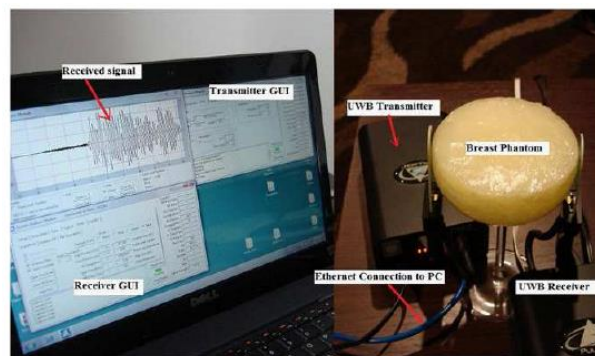


Fig. 12. Experimental setup used in [40]. Image is adapted from [40].

Porter, E et al. [41] have contributed in phantom development by creating heterogeneous phantoms for fat, skin, gland and tumor. Relative permittivity and conductivity of the each phantom were measured at microwave frequencies. They also described a proper methodology and procedure to merge four phantoms into a single hemispherical breast model. The final breast phantom comprised of 2 mm layer of skin enveloping a mixture of fat, gland and one or more tumors. It has a radius of 0.65 m with 0.015 m tumor inside the gland. The procedure that they used to mix the individual phantoms into a final breast model is summarized as follows. Complete list of the constituents with their amount of concentrations for each phantom type is provided in Table 11. Dielectric measurements at 4GHZ for individual phantoms are shown in Table 12. The final phantom produced is shown in Fig. 13.

Procedure of mixing individual phantoms into a final breast model in [41]:

- 1) Prepare a 2 mm thick skin phantom by pouring liquid skin mixture between two hemispherical bowls. Air bubbles must be avoided when skin mixture is compressed between the bowls. Therefore, skin mixture must be slowly poured in the space.
- 2) Give time to harden the mixture and after it, remove the bowls. Proper case must be taken when removing the bowls because otherwise this could cause tearing of skin phantom. To avoid this mishap, equal pressure must be applied from all sides when removing the bowls.
- 3) Once the skin is set, fat phantom could be poured directly into it.
- 4) Tumor models can now be placed at any location in the fat phantom, which is now inside skin phantom.
- 5) For positioning glands within the phantoms, cylindrical glass rods were anchored in the fat before it solidified.
- 6) After the hardening of fat phantom the rods were be removed and the remaining holes were carved out into a conical shape.
- 7) Then the liquid gland mixture was poured directly into the conical hole.
- 8) This technique permitted multiple gland models, and, allowed multiple tumors to be placed within the glands.

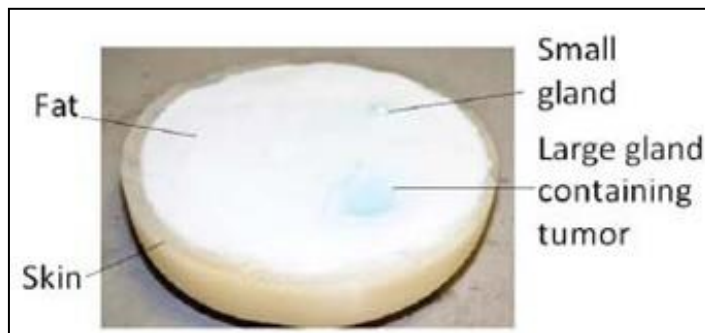


Fig. 13. Complete phantom model of breast developed in [41]. Image adapted from [41].

Table 11. List of the constituents for each phantom type as used in Emily Porter et al. [41].

	p-toulic acid (g)	n-propanol (mL)	Deionized water (mL)	200 Bloom Gelatin (g)	Formaldehyde (37% by water) (g)	Oil (mL)	Ultra Ivory Detergent (mL)
<b>Fat</b>	0.133	6.96	132.7	24.32	1.53	265.6	12.00
<b>Gland</b>	0.253	12.71	241.9	43.27	2.74	141.5	6.79
<b>Skin</b>	0.294	28.69	279.5	50.02	3.33	98.6	5.86
<b>Tumor</b>	0.346	17.00	328.0	58.67	3.72	38.4	2.00

Table 12. Dielectric measurements for each phantom type as used in Emily Porter et al. [41].

Breast part (Including Tumor)	Relative Permittivity 4 GHz	Conductivity (S/M) 4 GHz	Tumor Size Detected
<b>Skin</b>	33	2.4	2.5 mm
<b>Fat</b>	14.6	0.6	
<b>Gland</b>	32.2	1.7	
<b>Tumor</b>	53	3.5	

Santorelli, A. and Porter, E et al. [42] demonstrated an advanced time domain experimental system for microwave breast cancer detection using Synthesized Broadband Reflector SBR structure for pulse shaping. They used breast phantoms developed in [41] for experimentation purpose. In these phantoms both relative permittivity and conductivity were taken similar to those of the tissues that make up the breast anatomy. The experimental setup using this phantom is shown in Fig. 14. Apart of being an experimental system, the authors have not made a classification of tumor type in [41] and [42]. This is one of their shortcomings.

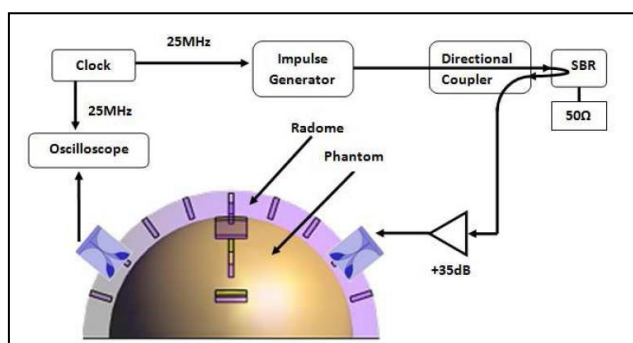


Fig. 14. Breast phantom of [41] in complete experimental setup for breast cancer detection system [42] Image adapted from [42].

Abdullah R.S.A. Raja et al. [43] provided a feasibility study of UWB (as the signal source) and microwave forward scattering (FSR) radar for breast cancer detection. In this work UWB Forward Scattering Radar Cross Section, FS RCS along with Doppler frequency profile was investigated at 3, 6 and 9 GHz center frequencies. The Doppler frequency existence is due to the fact of relative motion between the UWB signal source and the receiver. Results showed that cancerous breast has higher Doppler frequency value. A cylindrical and hemi ellipsoid shaped second order Debye model [32] was utilized to form the electromagnetic breast model, either with or without the presence of tumor.

Bakar, A.A et al [44] presented the design, implementation and testing of various mixtures for the development of a heterogeneous breast phantom for UWB microwave imaging. The implemented sample and the phantom were shown to cover a broad range of dielectric properties of healthy tissues from (relative permittivity) 6-48 across the frequency range of 3 GHz to 11 GHz. In addition to this, breast phantoms mimicking the variation of density of woman's breast with contrast to dielectric constant between cancerous and healthy tissue could be obtained by the presented designs. One of their contributions was the making of low dense and high dense breast phantoms categorically.

**For low dense breast** the constituents used in [44] were; 12 g propylene glycol, 193 milli-Q water, 30.8 g gelatin, 200 mL of grape seed oil, 2.2 mL of commercial dishing water liquid an 1.512g of formalin solution. For cross linking agent, Glyxal and Glutaraldehyde were used because of their higher dielectric constant values. Milli Q is trademark used by Millipore Corporation to describe ultrapure water of Type 1 (ISO 3696) [45]. It shows high quality of purification and deionization.

**For dense phantom in** [44], 7 g of agar powder, 30 mL of vegetable oil and 2 mL of dishwashing liquid is mixed into 450 mL of deionized water.

Dehydration in these phantoms was controlled by wrapping the phantoms with a cling wrap and molding them in Pyrex glass. Complex permittivity was measured by HP 85070A connected to an open ended coaxial probe, after proper calibration Table 8 presents the summary of the results in [44], as a comparison, of dielectric constant of phantom samples and real tissues.

Table 13. Dielectric properties of phantoms measured at 7.5 GHz. in [33].

Breast Type/ Part	Relative Permittivity @ 7.5 GHz		RMS Error
	Real Tissue	Phantom	
Low Density	6.90	6.94	1.22
		7.949	2.59
High Density	39.77	41.82	2.89

Bakar, A.A [46] presented ultra-wideband microwave imaging system in terms of slot antennas and heterogeneous breast phantoms developments are discussed for the development of an. In terms of dielectric properties fabricated breast phantoms behave very much like real breasts. Using [44] dense and low dense breast phantoms were prepared. The acquired results indicated the possibility of detecting small tumors. In order to have stable dielectric properties, lasting for longer durations agar based material was selected in the fabrication of phantoms. The UWB imaging system with phantom picture is shown in Fig. 15.

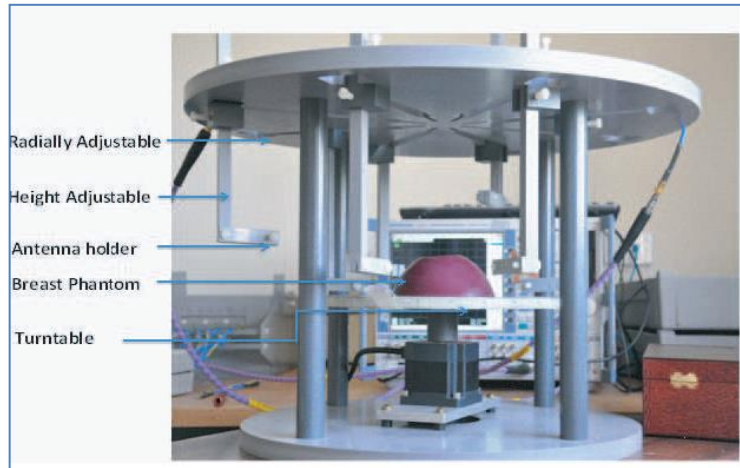


Fig. 15. Complete experimental setup using phantoms in [46]. Image adapted from [46].

Tiang.S.S et al [47] has presented design and fabrication of biconical antenna has which gives reflection coefficient in the UWB impedance bandwidth. Both homogeneous and heterogeneous breast phantoms were used with this antenna array with the aim of early breast cancer detection. Image reconstruction was then performed with the received signal with the proposed algorithm. To experiment the procedures the homogeneous fatty and heterogeneous glandular models were created using chemical materials which were devised based on the relative permittivity and conductivity of realistic tissue over the frequency of interest. All materials that were used were dispersive. The breast phantom size was fabricated simulating 76 mm diameter fatty tissue with 2 mm thick skin layer with glandular structures that are heterogeneously distributed. The chemicals were mixed and molded into an 80 mm hemispherical shape, forming the breast phantom. The tumor with permittivity of 54 was molded into cylindrical shape rod with 5 mm diameter and inserted vertically inside the glandular area as described in [41]. Figures 16(a) and 16(b) show the resulting homogenous and heterogeneously glandular breast phantoms. Table 14 shows the relative permittivity and conductivity values for the manufactured phantoms.

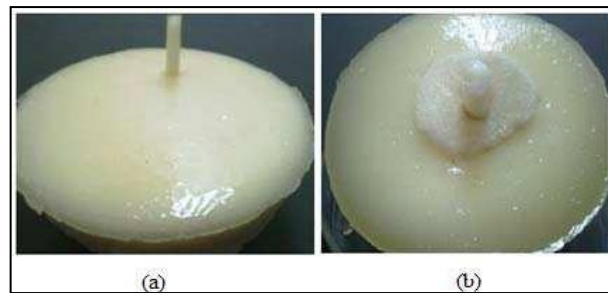


Fig. 16. Phantoms used in [47], (a) homogeneous breast phantom. (b) heterogeneous breast phantom. Images adapted from [47].

Table 14. Summary of relative permittivity values used in [35] in phantoms.

Tissue Type	Relative Permittivity @ 4.5 GHz	Conductivity (S/m)	Tumor Size Detected
Fat	11-18	0.1-0.2	5mm
Skin	33-46	0.15-3.8	
Glandular	28-40	0.1-3.0	
Tumor	48-66	0.15-5.0	

In [48] Klemm et al. marked for the first time experimental work on microwave breast cancer imaging using inhomogeneous breast phantoms. A 31-antenna array was used in imaging experiments. The imaging

system operated in the full ultrawideband frequency range, between 3 and 10 GHz. To verify imaging performance of that system, new breast phantoms with inhomogeneous internal structure were developed. For three different breast phantoms presented in [52], the contrast between spherical phantom tumors and surrounding materials ranged from 5:1 to 1.6:1. The results showed that the biggest challenge in radar microwave imaging was the inhomogeneity of the volume being sensed, and not the contrast itself. In addition to experimental results, the authors also presented the new image formation algorithm, which was a modified version of the delay-and-sum (DAS) algorithm. The new algorithm proved effective in reducing clutter, providing better images. The new algorithm improved the peak clutter-to-target energy ratio by 3.1 dB.

Michaelsen, Kelly E., et al [49] focused on the design and development of anthropomorphic breast phantoms with physiological water, lipid, and hemoglobin content for near-infrared spectral tomography. Phantom measurements have certainly been an important part of the development of near-infrared (NIR) spectral tomography (NIRST). NIR light (600 to 1000 nm) is absorbed by hemoglobin, water, and lipids—tissue chromophores that are often altered in the presence of malignancy. This is a very important scenario to determine the presence of tumors. The phantoms developed in [49] were long-lasting and demonstrated water and lipid fractions that were consistent to within 5% of their original content measured 2 weeks after their formation. A breast-shaped three-layered model of adipose, fibroglandular, and malignant tissues was created with water content ranging from 30% for the adipose simulant to 80% for the tumor. Skin was not included in the layered structure, unlike the previous work on phantom. Mean measured water content ranged from 30% in simulated adipose to 73% in simulated tumor with the higher water localized to the tumor-like material. This matched with the results obtained in earlier phantom study. The demonstrated heterogeneous phantom design was composed of physiologically relevant concentrations of the major optical absorbers in the breast in the near-infrared wavelengths that significantly improved imaging system characterization and optimization because the materials have stand-alone structural integrity and can be readily moulded into the sizes and shapes of tissues commensurate with clinical breast imaging.

Joachimowicz, Nadine, et al [50] studied the dielectric properties of various mixtures vulnerable to be used in manufacturing of reference heterogeneous breast phantoms devoted to the experimental validation of microwave breast imaging systems in the 0.5–6-GHz frequency range, i.e. lower end of UWB range. Predominantly, authors investigated the steadiness over time and temperature of the mixtures' properties and their reproducibility, along with the ability of the mixtures to impersonate the various breast tissues, i.e., to show dielectric properties close to that given by one-pole Debye models that describe the mean relative dielectric permittivity of various tissue types. In their conclusion, the authors concluded about the comparison of two types of mixtures. The first type of mixture, made of oil and gelatin, is exigent to preserve over very long periods of time, whereas the second one, made of water, Triton X-100, and salt, is proven to be a good candidate for the realization of such phantoms, as these mixtures are easy to produce, and their electromagnetic parameters are stable over temperature and over very long time periods.

Research in [51] presented a theoretical model to determine absolute permittivity values of glandular breast tissue with close approximation. Experimental permittivity values were compared with Debye 1st order/ single pole theoretical results to find errors/ mismatching for 1GHz to 6 GHz Ultra-Wide Band (UWB) frequencies. Least square fitting was then employed for error reduction. Projected estimation model showed the capacity to lessen the gap 19.28% and 41.20% for healthy and malignant breast tissues respectively. Further, a methodology was also developed and proposed for predicting absolute permittivity values for experimental breast phantoms for other frequencies of 7GHz, 8GHz, 9GHz and 10GHz which are not available so far for normal and tumor containing cases for breast tissue cancer.

## 7. Numerical Breast Phantoms (Computer Models)

Computational Electromagnetic techniques are commonly used to model the propagation of EM waves in materials and in biological tissues. One of such techniques is Finite Difference Time Domain (FDTD) method. FDTD is able to provide dielectric properties of the constituent tissues and their associated distribution in the breast. A good FDTD algorithm requires the physical geometry of the breast, its heterogeneity and dispersive nature and a suitable imaging system as in input. An imaging system describes the orientation of the patient and positions of the antenna. O' Halloran, M et al. [52] presented a comprehensive review of the dielectric properties of normal and diseased (cancerous) breast tissues, the heterogeneity of the normal breast tissue with respect to FDTD usage to make a numerical model. In this

review paper the authors have contributed an inclusive review and comparison of FDTD 2D breast phantom models with those that are of 3D FDTD.

Xie et al. [53] took into consideration adaptive multi-static microwave imaging for breast cancer detection in a simulated FDTD environment. An antenna array was used, in which one of the antenna was transmitting through a 3D breast model and other were receiving the backscattered pulse. The dielectric properties used in [49] for breast phantoms are given in Table 15. The cross-section of FDTD 3D hemisphere breast model is shown in Figs. 17 and 18.

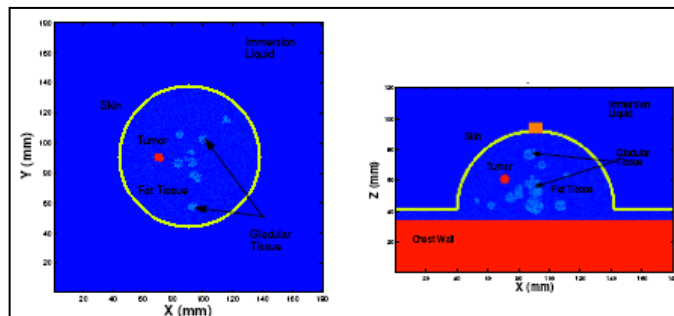


Fig. 17. Cross-section of 3D breast model. Image adapted from [53].

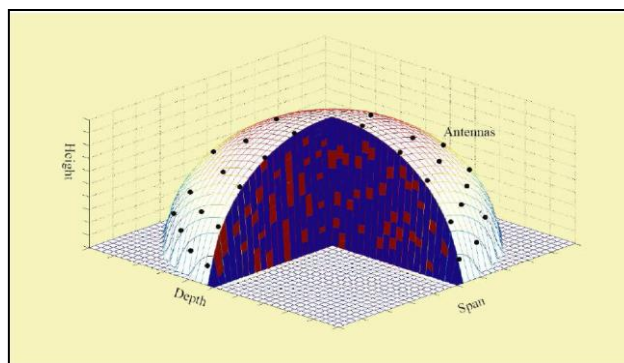


Fig. 18. 3D view of hemispherical breast model developed by Xie et al [53]. Image is taken from [53].

Table 15. Dielectric properties of breast tissue used in Xie’s FDTD model [53].

Tissue Type	Relative Permittivity	Conductivity	Tumor Size Detected
Immersion Liquid	9	0	
Fatty Breast Tissue	9	0.4	
Chest Wall	50	7	
Skin	36	4	6mm and 4mm
Nipple	45	5	
Glandular Tissue	11-15	0.4-0.5	
Tumor	50	4	

Zastrow, et al. [54], accounted the development of different shapes, size and radiographic density, anatomically realistic 3-D numerical breast phantoms can conveniently be used in finite-difference time-domain computational electromagnetics (FDTD) models. For MRI in addition to tissue density, tissue relaxation properties contribute to image contrast in them. There are two types of relaxation properties: T1 relaxation and T2 relaxation. The phantoms in [54] were based on T1-weighted MRIs of prone patients. The technique employed was, each MRI was transformed into a uniform grid of dielectric properties using. First, the structure of each phantom was identified by applying image processing techniques to the MRI. Next, the voxel intensities of the MRI are converted to frequency-dependent and tissue-dependent

dielectric properties of normal breast tissues via a piecewise-linear map. While Cole–Cole models provide a compact, general representation of the dispersive dielectric properties of breast tissue, they were difficult to be included into wideband FDTD simulations. The Cole–Cole models were replaced by simple Debye model and that has shown to precisely incarcerate the frequency dependence of these properties in the microwave frequency range.

Conceicao, R et al [55] provided a foundation for the improvement of better geometrically and dielectrically accurate numerical breast phantoms with implanted tumors. The paper examines the anatomy and physiology of the breast and the growth of breast cancer. This paper examined types of breast tumors, their formation at cellular level. Dielectric properties are also reviewed. Modeling techniques are also reviewed, describing how MRI data is mapped to FDTD breast phantoms. They have presented an FDTD model integrating pragmatic tumor models with the focus of breast heterogeneity. Tumor modeling was accomplished using polygonal approximation for 2D case and Gaussian Random Spheres for 3D case. The phantoms were formed by using 3D MRI's of the breast. For each MRI of breast, each voxel was mapped with accurate dielectric properties in the FDTD phantom. Breast models were categorized on the basis of percentage difference of adipose and glandular tissues into dense and low dense types. Single pole Debye model, was used to obtain dispersive nature of breasts. Uniaxial Perfectly Matched Layer (UPML) was used to define boundary terminations of the phantoms. They provide minimum edge reflections.

Kiarashi, Nooshin, et al. [56] identified the key consequences of anatomy on image quality and clinical performance. Currently, there is no commercially available three-dimensional physical breast phantom that is anthropomorphic. The authors presented the development of a new set of physical breast phantoms based on human data. The phantoms were designed to match the extended cardiac-torso virtual breast phantoms that were based on dedicated breast computed tomography images of human subjects. The phantoms were fabricated by high-resolution multimaterial additive manufacturing (3D printing) technology. Based on the current state-of-the-art in the technology and available materials, two variations were fabricated. The first was a dual-material phantom, the Doublet. Fibroglandular tissue and skin were represented by the most radio graphically dense material available; adipose tissue was represented by the least radio graphically dense material. The second variation, the Singlet, was fabricated with a single material to represent fibroglandular tissue and skin. It was subsequently filled with adipose-equivalent materials including oil, beeswax, and permanent urethane-based polymer. Simulated micro-calcification clusters were further included in the phantoms via crushed eggshells. The phantoms were imaged and characterized visually and quantitatively. The mammograms of the phantoms demonstrated close correlation with simulated mammographic projection images of the corresponding virtual phantoms.

## 8. Conclusion

Phantoms play an imperative role in the development, validation, and quality control of imaging systems. Clinically, they are recommended for quality management or mandated for technical surveillance to avoid system malfunction and possible adverse effects on patients undergoing examination. In research and development, phantoms are used for early-stage feasibility testing and performance evaluation; they assist in diagnosing errors or underperforming instrumentation, and enable comparisons of data acquired on different imaging systems.

The purpose of this paper was to provide a survey on mathematical formulations for dielectric measurements and how research been traversed in the past decade to use them for making hardware breast phantoms. In is studied that mostly commonly used model for dielectric properties of human breast tissues is single pole Debye models. Cole-Cole models do provide more accurate results but they are difficult to be incorporated because of complex solutions.

Computational electromagnetics models of microwave interactions with the human breast serve as an invaluable tool for exploring the feasibility of new technologies and improving design concepts related to microwave breast cancer detection and treatment.

In addition to physically realizable breast phantoms we have also provided a small review on numerical breast phantoms as well. Most commonly employed algorithm is Finite Difference Time Domain (FDTD) approach. Numerical phantoms acquire the structural heterogeneity of the breast tissue, integrating the dispersive characteristics. The high permittivity values of the glandular structure can be readily included along with tumor properties in them.

The layered structure used to define human breast along with the survey and review provided in this paper can be used in the future research for developing body propagation model for human breast tissue.

Consequently this could be used to define channel impulse response for a UWB breast cancer transceiver communication and imaging system.

## References

- [1] J. Mitteldorf. (2013, April 8). *The Immune System Protects Us against Cancer (Revised ed.)* [Online]. Available: <http://joshmitteldorf.scienceblog.com/2013/04/08/the-immune-system-protects-us-against-cancer/>
- [2] American Cancer Society. (2013, Feb 26). *Breast Cancer* [Online]. Available: <http://www.cancer.org/acs/groups/cid/documents/webcontent/003090-pdf.pdf>
- [3] Komen®. (2012, October 22). *Benign Breast Conditions (Updated ed.)* [Online]. Available: <http://ww5.komen.org/BreastCancer/BenignConditions.html>
- [4] L. C. Hartmann, T. A. Sellers, M. H. Frost, W. L. Lingle, A. C. Degnim, K. Ghosh, R. A. Vierkant, S.D. Maloney, V. S. Pankratz, D. W. Hillman, and V. J. Suman, "Benign breast disease and the risk of breast cancer," *New England Journal of Medicine*, vol. 353, no. 3, pp. 229-237, 2005.
- [5] J. A. Ligibel. (2005, June 1). *Breast Cancer Metastasis (Updated ed.)* [Online]. Available: <http://www.healthcentral.com/encyclopedia/408/484.html?ref=wusa9.com>
- [6] H. Vainio and F. Bianchini, "Screening techniques," in *Breast Cancer Screening*, vol. 7, 1st ed. Lyon, France: IARC Press, 2002, pp. 25-37.
- [7] Breast.cancer.org. (2012, Sept. 17). *Chest X-Rays (Modified ed.)* [Online]. Available: <http://www.breastcancer.org/symptoms/testing/types/xray>
- [8] Breast.cancer.org. (2012, Sept. 17). *Breast MRI (Modified ed.)* [Online]. Available: <http://www.breastcancer.org/symptoms/testing/types/mri>
- [9] Breast.cancer.org. (2012, Nov. 1). *Ultrasound (Updated ed.)* [Online]. Available: <http://www.breastcancer.org/symptoms/testing/types/ultrasound>
- [10] X. Li, S. K. Davis, S. C. Hagness, D. W. van der Weide, and B. D. Van Veen, "Microwave imaging via space-time beamforming: Experimental investigation of tumor detection in multilayer breast phantoms," *Microwave Theory and Techniques, IEEE Transactions on*, vol. 52, no. 8, pp. 1856-1865, Aug. 2004.
- [11] X. Xiao and T. Kikkawa, "Study on the breast cancer detection by UWB microwave imaging," in *Microwave and Millimeter Wave Technology, 2008. ICMMT 2008. International Conference on*, 21-24 April 2008, vol. 4, pp. 1707-1710.
- [12] G. Bindu, A. Lonappan, V. Thomas, C. K. Anandan, and K. T. Mathew, "Active microwave imaging for breast cancer detection," *Progress In Electromagnetics Research*, vol. 58, pp. 149-169, 2006.
- [13] L. Sha, E. R. Ward, and B. Stroy, "A review of dielectric properties of normal and malignant breast tissue," in *SoutheastCon, 2002. Proceedings IEEE*, 2002, pp. 457-462.
- [14] M. Lazebnik, L. McCartney, D. Popovic, C. B. Watkins, M. J. Lindstrom, J. Harter, S. Sewall, A. Magliocco, J. H. Booske, M. Okoniewski, and S. C. Hagness, "A large-scale study of the ultrawideband microwave dielectric properties of normal breast tissue obtained from reduction surgeries," *Physics in Medicine and Biology*, vol. 52, no. 10, pp. 2637-2656, 2007.
- [15] *The Loudoun Center of Plastic Surgery and Dermatology* [Online]. Available: <https://www.loudouncenterforplasticsurgery.com/virginia-breast-anatomy-augmentation/>
- [16] C. Wessel, J. A. Schnabel, and M. Brady, "Towards a more realistic biomechanical modelling of breast malignant tumours," *Physics in Medicine and Biology*, vol. 57, no. 3, pp. 631-648, Jan. 2012.
- [17] C. Gabriel, S. Gabriel, E. Corthout, "Compilation of the dielectric properties of body tissues at RF and microwave frequencies," Department of Physics, King's College London, UK, Tech. Rep. AL/OE-TR-1996-0037, Jun. 1996.
- [18] *Scilab Enterprises* [Online]. Available: <http://www.scilab.org>
- [19] P. Debye, *Ver. Deut. Phys. Gesell.*, vol. 15, 1913, p. 777; reprinted 1954 in collected papers of Peter J. W. Debye Interscience, New York.
- [20] D. K. Ghodgaonkar and A. B. Daud, "Calculation of Debye parameters of single Debye relaxation equation for human skin in vivo," in *Proceedings 4th National Conference on Telecommunication Technology, 2003, NCTT 2003*, 14-15 Jan. 2003, pp. 71-74.
- [21] K. Cole and R. Cole, "Dispersion and absorption in dielectrics I. Alternating current characteristics," *J. Chem. Phys.*, vol. 9, pp. 341-52, 1941.
- [22] D. Davidson and R. Cole, "Dielectric relaxation in glycerol, propylene glycol, and n-propanol," *J. Chem. Phys.*, vol. 19, pp. 1484-1490, 1951.

- [23] M. F. Causley and P. G. Petropoulos, "On the time-domain response of Havriliak-Negami dielectrics," *Antennas and Propagation, IEEE Transactions on*, vol. 61, no. 6, pp. 3182–3189, June 2013.
- [24] T. Said and V. V. Varadan, "Modeling the effective complex permittivity of heterogeneous breast tissue and comparison with relaxation models at millimeters wave frequencies," in *Region 5 Technical Conference, 2007 IEEE*, 20-22 April 2007, pp. 157–162.
- [25] G. Bindu, S. J. Abraham, C. K. Anandan, and K. T. Mathew, "Microwave characterization of female human breast tissues," in *Wireless Technology, 2006. The 9th European Conference on*, 10-12 Sept. 2006, pp. 123–126.
- [26] M. Cavagnaro, F. Frezza, R. Laurita, M. Tannino, L. Manganaro, M. Marini, P. Sollazzo, A. Stagnitti, V. Lopresto, and R. Pinto, "Water content evaluation of a human tissue using magnetic resonance imaging: A quantitative benchmarking approach," in *Electromagnetic Compatibility (EMC EUROPE), 2012 International Symposium on*, vol., 17-21 Sept. 2012, pp. 1-6.
- [27] S. Mashimo, S. Kuwabara, S. Yagihara, and K. Higasi, "Dielectric relaxation time and structure of bound water in biological materials," *J. Phys. Chem.*, vol. 91, pp. 6337–6338, Dec. 1987.
- [28] T. J. Walters, D. W. Blick, L. R. Johnson, E. R. Adair, and K. R. Foster, "Heating and pain sensation produced in human skin by millimeter waves: comparison to a simple thermal model," *Health Physics*, vol. 78, no. 3, pp. 259–267, Mar. 2000.
- [29] T. S. England, "Dielectric properties of the human body for wavelengths in the 1-10 cm range," *Nature*, vol. 166, pp. 480–481, Sept. 1950.
- [30] H. F. Cook, "The dielectric behaviour of some types of human tissues at microwave frequencies," *British J. Appl. Physics*, vol. 2, no. 10, pp. 295 – 300, Oct. 1951.
- [31] C. M. Alabaster, "Permittivity of human skin in millimeter wave band," *Electronics Letters*, vol. 39, no. 21, pp. 1521-1522, Oct. 2003.
- [32] C. M. Alabaster, "The microwave properties of tissue and other lossy dielectrics," Ph.D. thesis, Dept. of Aerospace, Power and Sensors, Cranfield University, College of Defence Tech., Bedfordshire MK43-0AL, United Kingdom, Mar. 2004
- [33] A. M. Campbell, "Measurements and analysis of the microwave dielectric properties of tissues," Ph.D. dissertation, University of Glasgow, UK, 1990.
- [34] M. Lazebnik, D. Popovic, L. McCartney, C. B. Watkins, M. J. Lindstrom, J. Harter, S. Sewall, T. Ogilvie, A. Magliocco, T. M. Breslin, and W. Temple, "A large scale study of the ultrawide band microwave dielectric properties of normal, benign and malignant breast tissues obtained from cancer surgeries," *Phys. Med. Biol.*, vol. 52, pp. 6093-6115, 2007.
- [35] M. Klemm, J. A. Leendertz, D. Gibbins, I. J. Craddock, A. Preece, and R. Benjamin, "Microwave radar-based breast cancer detection: Imaging in inhomogeneous breast phantoms," *Antennas and Wireless Propagation Letters, IEEE*, vol. 8, pp. 1349-1352, 2009.
- [36] J. C. Y. Lai, C. B. Soh, E. Gunawan, and K. S. Low, "Homogeneous and heterogeneous breast phantoms for ultra-wideband microwave imaging applications," *Progress In Electromagnetics Research, PIER*, vol. 100, pp. 397-415, 2010.
- [37] J. C. Y. Lai, C. B. Soh, E. Gunawan, and K. S. Low, "UWB microwave imaging for breast cancer detection—Experiments with heterogeneous breast phantoms," *Progress In Electromagnetics Research M*, vol. 16, pp. 19-29, 2011.
- [38] S. Alshehri, S. Khatun, and Z. Awang, "Homogeneous and heterogeneous breast phantoms for UWB imaging," in *ISABEL'11, Proceedings of the 4th International Symposium on Applied Sciences in Biomedical and Communication Technologies*, ACM, 2011, Barcelona, Spain, p. 1,
- [39] S. Alshehri and S. Khatun, "UWB imaging for breast cancer detection using neural network," *Progress In Electromagnetics Research C*, vol. 7, pp. 79–93, 2009.
- [40] S. A. AlShehri, S. Khatun, A. B. Jantan, R. S. A. Raja Abdullah, R. Mahmud, and Z. Awang, "Experimental breast tumor detection using NN-based UWB imaging," *Progress In Electromagnetics Research*, vol. 111, pp. 447-465, 2011.
- [41] E. Porter, A. Santorelli, A. Coates, and M. Popovic, "An experimental system for time-domain microwave breast imaging," in *Proc. 5th European Conference on Antennas and Propagation (EUCAP 2011)*, Rome, Italy, Apr. 11-15, 2011.
- [42] A. Santorelli, M. Chudzi, E. Kirshin, E. Porter, A. Lujambio, I. Arnedo, M. Popovi, and J. Schwartz, "Experimental demonstration of pulse shaping for time-domain microwave breast imaging," *Progress In Electromagnetics Research*, vol. 133, pp. 309-329, 2013.

- [43] R. S. A. Raja Abdullah, O. N. Samijayani, S. Adabi, A. Ismail, M. I. Saripan, and S. A. Alshehri, "Breast tumor detection using microwave ultra wideband (UWB) forward scattering radar system," *International Journal of Physical Sciences*, vol. 7, no. 46, pp. 6062-6074, Dec. 2012.
- [44] A. A. Bakar, A. Abbosh, and M. Bialkowski, "Fabrication and characterization of a heterogeneous breast phantom for testing an ultrawideband microwave imaging system," in *Microwave Conference Proceedings (APMC), 2011 Asia-Pacific*, pp. 1414-1417.
- [45] *Water for Analytical Laboratory Use*, ISO Standard 3696, 1987.
- [46] A. A. Bakar, D. Ireland, A. Abbosh, and Y. Wang, "Experimental assessment of microwave diagnostic tool for ultra-wideband breast cancer detection," *Progress In Electromagnetics Research M*, vol. 23, pp. 109-121, 2012.
- [47] S. S. Tiang, M. Sadoon, T. F. Zanoon, M. F. Ain, and M. Z. Abdullah, "Radar sensing featuring biconical antenna and enhanced delay and sum algorithm for early stage breast cancer detection," *Progress In Electromagnetics Research B*, vol. 46, pp. 299-316, 2013.
- [48] M. Klemm, J. A. Leendertz, D. Gibbins, I. J. Craddock, A. Preece, and Ralph Benjamin, "Microwave radar-based differential breast cancer imaging: Imaging in homogeneous breast phantoms and low contrast scenarios," *IEEE Transactions on Antennas and Propagation*, vol. 58, no. 7, pp. 2337-2344, 2010.
- [49] K. E. Michaelsen, V. Krishnaswamy, A. Shenoy, E. Jordan, B. W. Pogue, and K. D. Paulsen, "Anthropomorphic breast phantoms with physiological water, lipid, and hemoglobin content for near-infrared spectral tomography," *Journal of Biomedical Optics*, vol. 19, no. 2, pp. 026012-026012, 2014.
- [50] N. Joachimowicz, C. Conessa, T. Henriksson, and B. Duchêne, "Breast phantoms for microwave imaging," *IEEE Antennas and Wireless Propagation Letters*, vol. 13, pp. 1333-1336, 2014.
- [51] I. E. Khuda, "Estimation modeling of heterogeneous tissue permittivity for developing tissue phantoms," *Sci. Int. (Lahore)*, vol. 28, no. 4, pp. 3939-3945, 2016.
- [52] M. O'Halloran, R. Conceicao, D. Byrne, M. Glavin, and E. Jones, "FDTD modeling of the breast: A review," *Progress in Electromagnetics Research B*, vol. 18, pp. 1-24, 2009.
- [53] Y. Xie, B. Guo, L. Xu, J. Li, and P. Stoica, "Multistatic adaptive microwave imaging for early breast cancer detection," *IEEE Transactions on Biomedical Engineering*, vol. 53, no. 8, pp. 1647-1657, Aug. 2006.
- [54] E. Zastrow, S. K. Davis, M. Lazebnik, F. Kelcz, B. D. Van Veen, and S. C. Hagness, "Development of anatomically realistic numerical breast phantoms with accurate dielectric properties for modeling microwave interactions with the human breast," *IEEE Transactions on Biomedical Engineering*, vol. 55, no. 12, pp. 2792-2800, 2008.
- [55] R. Conceicao, M. O'Halloran, M. Glavin, and E. Jones, "Numerical modeling for ultra wideband radar breast cancer detection and classification," *Progress in Electromagnetics Research B*, vol. 34, pp. 145-171, 2011.
- [56] N. Kiarashi, A. C. Nolte, G. M. Sturgeon, W. P. Segars, S. V. Ghate, L. W. Nolte, E. Samei, and J. Y. Lo, "Development of realistic physical breast phantoms matched to virtual breast phantoms based on human subject data," *Medical Physics*, vol. 42, no. 7, pp. 4116-4126, 2015.